Appl Phys A
DOI 10.1007/s00339-008-4881-8

Applied Physics A
Materials Science & Processing

Cobalt iron-oxide nanoparticle modified poly(methyl methacrylate) nanodielectrics

Dielectric and electrical insulation properties

Enis Tuncer · Adam J. Rondinone · Jonathan Woodward · Isidor Sauers · D. Randy James · Alvin R. Ellis

Received: 16 June 2008
© Springer-Verlag 2008

Abstract In this paper, we report the dielectric properties of composite systems (nanodielectrics) made of small amounts of mono dispersed magnetic nanoparticles embedded in a polymer matrix. It is observed from the transmission electron microscope images that the matrix polymeric material is confined in approximately 100 nm size cages between particle clusters. The particle clusters are composed of separated spherical particles which comprise unconnected networks in the matrix. The dielectric relaxation and breakdown characteristics of the matrix polymeric material are altered with the addition of nanometer size cobalt iron-oxide particles. The dielectric breakdown measurements performed at 77 K showed that these nanodielectrics are potentially useful as an electrical insulation material for cryogenic high voltage applications. Finally, structural and dielectric properties of nanocomposite dielectrics are discussed to present plausible reasons for the observed low effective dielectric permittivity values in the present and similar nanodielectric systems. It is concluded that polymeric nanoparticle composites would have low dielectric permittivity regardless of the permittivity of nanoparticles are when the particles are coordinated with a low dielectric permittivity surfactant.

PACS 61.46.-w · 82.35.Np · 77.22.Jp · 77.22.Gm

The research was sponsored by three different sources: (i) the Laboratory Directed Research and Development (LDRD) Program of Oak Ridge National Laboratory (ORNL), managed by UT-Battelle, LLC for the U.S. Department of Energy under Contract No. DE-AC05-00OR22725 (D06-100), (ii) by the U.S. Department of Energy, Office of Electricity Delivery and Energy Reliability, Superconductivity Program for Electric Power Systems, under contract No. DE-AC05-00OR22725 with UT-Battelle, LLC, and (iii) by the Scientific User Facilities Division, Office of Basic Energy Sciences, U.S. Department of Energy.

E. Tuncer (✉) · I. Sauers · D.R. James · A.R. Ellis
Applied Superconductivity Group, Fusion Energy Division, Oak Ridge National Laboratory, Oak Ridge, TN 37831-6122, USA
e-mail: tuncere@ornl.gov

A.J. Rondinone
Neutron Nanoscience & Characterization, Center for Nanophase Materials Sciences Division, Oak Ridge National Laboratory, Oak Ridge, TN 37831-6494, USA

J. Woodward
Nanomaterials Chemistry Group, Chemical Sciences Division, Oak Ridge National Laboratory, Oak Ridge, TN 37831-6201, USA

Electrical insulation materials with improved physical properties are needed for high voltage applications, especially at cryogenic temperatures. To achieve such improvements material combinations in the form of nanocomposites have been investigated [1–4], other nanodielectric systems for conventional applications have also been reported [5–11]. This new class of materials, called *nanodielectrics*, exhibits promising results such that employed nanometer size inclusions have not degraded the dielectric properties of the matrix material. In addition, the lifetime of the electrical insulation systems have been improved significantly. There have been reports related to the lowering of the dielectric permittivity in some nanocomposites systems [12], which were related to the interaction zone or, in other words, the constraining of the polymer chain mobility [2, 5, 6, 13, 14]. Investigations into the properties of the interaction zones different polymeric systems relaxation dynamics in polymeric systems and their composites have been explained by nanoconfinement [15–18]. In the present study we particularly investigate this aspect of a nanocomposite system composed of

poly(methyl methacrylate) (PMMA) filled with cobalt iron-oxide ($CoFe_2O_4$) nanoparticles with dielectric spectroscopy and numerical simulations based on effective medium approach [19–21]. The dielectric properties, i.e., dielectric dispersion, non-linear low frequency response and dielectric breakdown strengths are reported to illustrate the potential of these systems in high voltage technology and power apparatus design. It is observed that the nanocomposites perform better than the unfilled matrix material in a cryogenic electrical insulation application.

The experimental details are as follows. The PMMA polymer was supplied from Sigma-Aldrich, and had a molecular weight of 996 000. PMMA was diluted with toluene 1:10 for synthesizing nano-composites. Co(acetylacetonate)$_3$ (98%), Fe(acetylacetonate)$_3$ (97%), 1,2-hexadecanediol (90%), oleic acid (90%), and oleylamine (70%) were purchased from Aldrich. Phenyl ether (99%) was purchased from Acros Organics. Hexane (99.5%) and denatured ethanol (90.5%) were purchased from Fisher. All reagents were used without further purification. Synthesis of 6 nm diameter $CoFe_2O_4$ nanoparticles was as follows [22]. The reagents Co(acac)$_3$ (0.356 g, 1 mmol), Fe(acac)$_3$ (0.706 g, 2 mmol), 1,2-hexadecanediol (2.58 g, 10 mmol), oleic acid (1.6 g, 6 mmol), oleylamine (1.61 g, 6 mmol), and phenyl ether (20 mL) were magnetically stirred and heated to 100°C under vacuum, then to 200°C under an Ar atmosphere and held at that temperature for 2 hours (acac = acetylacetonate). The reaction mixture was then heated to reflux (265°C) for an additional 1 hour under an Ar atmosphere and subsequently cooled to room temperature. Ethanol (40 mL) was added to the reaction mixture precipitating a black powder which was separated by centrifugation at 7500 rpm for 5 minutes. The product was then dissolved in 10 mL of hexane containing oleic acid (0.05 mL) and oleylamine (0.05 mL) and centrifuged at 6000 rpm for 10 minutes, discarding any undissolved residue. The black-colored product was precipitated with ethanol and purified twice by redissolving in hexane, centrifuging at 7500 rpm for 5 minutes, and precipitating with ethanol. Finally, PMMA/toluene mixture and $CoFe_2O_4$ were mixed in desired amounts to fabricate the samples. The mixtures were sonicated using a horn homogenizer for 15 min. Samples were cast on glass slides with thicknesses around 30 µm.

Structural properties and distribution of particles, homogenization, were investigated with the scanning transmission electron microscope (STEM, Hitachi HD-2000), which operated in bright field and Z-contrast STEM mode. The TEM samples were prepared by cutting off a small piece of the film, wetting in isopropanol, and placing on a 3 mm copper grid with carbon/formvar backing (Ted Pella, #1822). The impedance measurements were performed with a QuadTech 1920 LCR meter over 20 Hz–1 MHz frequency window at room temperature. Low frequency non-linear dielectric measurements were designed using a Keithley 6417A electrometer/high resistance meter. In these measurement a triangular source voltage was generated from the internal power supply of the electrometer using the Labview data acquisition program with oscillation frequency lower than 0.01 Hz. Breakdown tests were performed in a liquid nitrogen bath using a 20 kV transformer.

In Fig. 1, the TEM images of one of the samples are presented at different scaling/magnification levels. It is clear that at the low magnification image, Fig. 1a, that the particles are aggregated and formed clusters of approximately 100 nm in size. Although the sonication helps to disperse the particles, aggregates are still visible. As the magnification is increased, cf. Fig. 1b, individual particles are identified as bright gray spots, a clear separation between particles is visible. At the highest magnification, Fig. 1c, individual particles can be distinguished with particle sizes ranging between 5–10 nm, average particle size is around 6 nm. There is no connectivity between particles. The particles are coordinated (covered) with oleic acid, which is the surfactant. The distance between particles is several nanometers, the thickness of the surfactant. The $CoFe_2O_4$ particles have very narrow size distribution compared to our previous investigations [1, 2]. However, the aggregation is similar to the epoxy system studied [2], which indicate that the ex-situ particle fabrication and dispersing with sonication would not improve particle distribution. In the previously studied system [2] nanoparticles were larger than in the present case, and they were not functionalized with surfactants. Therefore, it is anticipated that the electric field enhancement and field grading effects would be better than that system. Although using capping agents and surfactants have been shown to improve particle dispersion, it is anticipated that the polarization and conduction properties of nanocomposites would be much different in the presence of those agents. The polarization and conduction characteristics of the agent should be known, i.e., an agent with high dielectric permittivity would not be beneficial for electrical insulation applications (as discussed below). Investigations on dielectric properties of the deionized water and water/octane mixture system, in which the water is dispersed as nanometer size spheres using a surfactant (butanol and cetyl trimethyl ammonium bromide) with reverse-micelles technique, showed that the presence of a surfactant alters the dielectric relaxation of octane–water mixture significantly.

Observe that in Fig. 1a the distance between particle clusters is around 100 nm. A perfectly uniform distribution on a basic cubic lattice with 6 nm particle size yields a spacing of around 30 nm, see Fig. 2. A regular distribution of particles would lead to a decrease in the number of nanoparticles. This would also yield an important breakthrough in designing nanocomposites with well defined structures and properties.

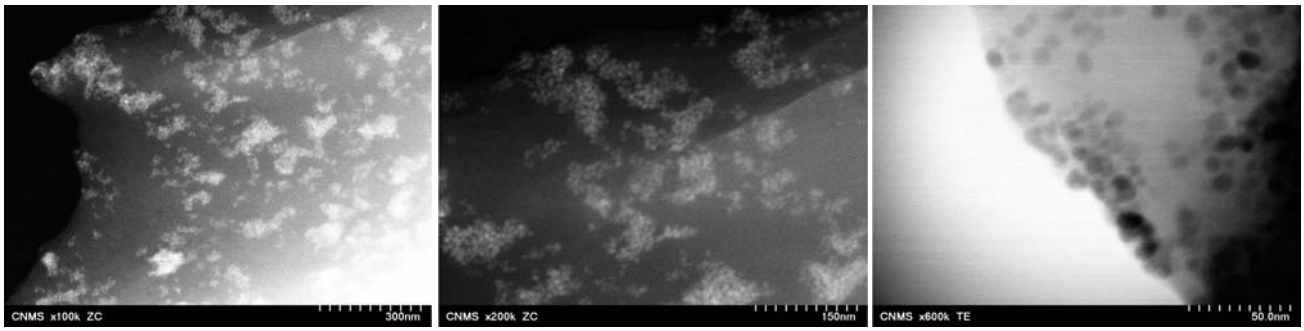

a **b** **c**

Fig. 1 Transmission electron microscope images of one of the samples with 2 vol% $CoFe_2O_4$. The images illustrate features at the different levels of magnification, **a** 300 nm, **b** 150 nm, and **c** 50 nm. In **a** and **b**, the *dark gray* regions are the poly(methyl methacrylate) and the *light* regions are the cobalt iron-oxide particles. In **c**, the particles are the *dark round objects*, and the polymer is the *light gray* background. In **a** and **b**, it is evident that a clump of particles are present. From **c** the average particle diameter can be estimated at around 6 nm

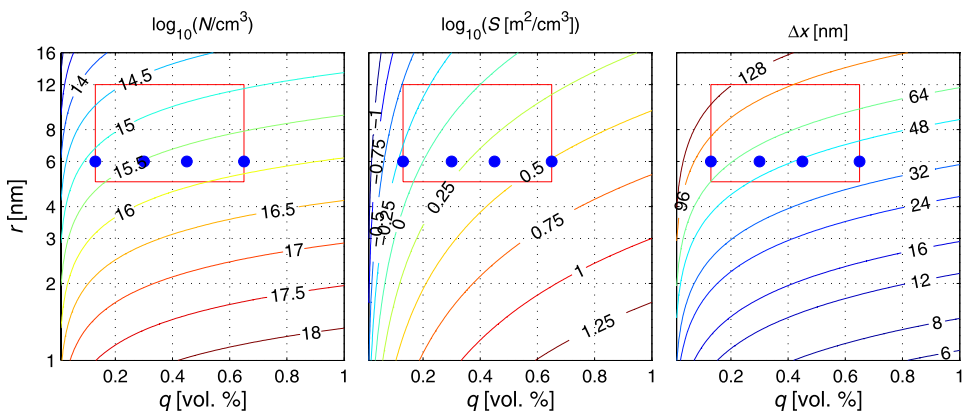

Fig. 2 Some physical quantities estimated for a nanoparticle filled composite. The calculations are performed assuming a basic cubic arrangement of particles. Volume fraction of particles q and particle radius r are varied. The particle number density N and total particle surface area S are presented per cm^3 of nanocomposite in contour plots. The distance between particles Δx are also shown to give a rough idea on the expected distance between particles in a nanocomposite. The rectangular area illustrates the expected parameter space for the studied systems due to particle size distribution, to pinpoint the location of the mixtures data are plotted with *filled symbols* (•). The fabricated $CoFe_2O_4$ PMMA systems with low concentration of nanoparticles could have the following structural properties $3 \times 10^{14}-10^{16}$ particles/cm^3, 0.3–4 m^2/cm^3 as the total particle surface area per cm^3 and 32–128 nm between particles

Although the particles form clumps, they do not fuse together forming large crystallites because of the utilized surfactant. In addition, the PMMA is forced between the particle clusters (confined in nano scale), constraining its molecular motion [15–18]. As an analogy to this phenomenon, assume a group of people apart from each other with their hands open and rotating on a field. If the poles are distributed randomly on the field, some of the crowd would not continue to rotate and their motion would be constrained leading to a decrease in the total rotational energy of the crowd. Similarly, the dielectric polarizability (or the polarization energy) of polymer chains would be constrained and the total polarization/permittivity of the polymer will be lowered in the presence of nanoparticles. Therefore, low permittivity values are obtained in nanodielectrics when compared to the permittivity of the matrix material. One should also consider the influence of the particles on the effective dielectric permittivity of the composite such that high permittivity material would increase the permittivity of the matrix. However, as will be shown later this does not have any significant influence on the permittivity of the composite when the particles are clearly separated.

In Fig. 3, the complex dielectric permittivity, $\varepsilon = \varepsilon' - \imath\varepsilon''$, of unfilled PMMA and $CoFe_2O_4$ filled PMMA are presented for the low voltage impedance measurements (applied voltage was 1 V). It is very clear that the dielectric dispersion of the PMMA is changed with addition of very low volume fraction of $CoFe_2O_4$ nanoparticles. The unfilled PMMA indicates a near-dc dielectric dispersion at frequencies lower than 1 kHz, where both the real and the imaginary parts

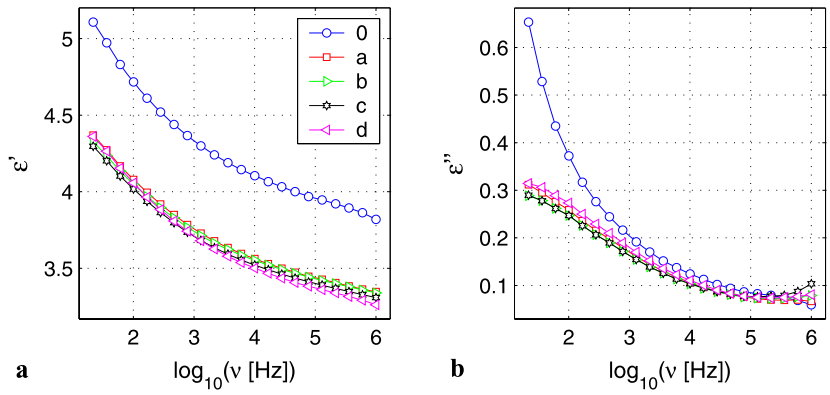

Fig. 3 **a** The real and **b** the imaginary parts of the complex dielectric permittivity of PMMA and PMMA-$CoFe_2O_4$ mixtures. The legends 0–d are the samples with different volume fraction of $CoFe_2O_4$, listed in Table 1. The lines are drawn to guide the eyes

Table 1 Dielectric properties of unfilled and $CoFe_2O_4$ filled PMMA. The weight and volume percentages of $CoFe_2O_4$ together with the high frequency permittivity ε_∞ and dc conductivity σ_0 values calculated from the DRT approach are listed. The data containing dielectric breakdown information are summarized. The mean and the standard deviations in the breakdown measurements are denoted with μ

Label	wt %	vol %	ε_∞ ϵ_0	σ_0 [pS/m]	b	a [kV/mm]	a_1 [kV/mm]	x_W [kV/mm]	x_G [kV/mm]	μ [kV/mm]
0	0	0	3.79	66.2	4.28	152.9	52.3	0.0	33.1	139 ± 36
a	0.60	0.13	2.89	8.81	4.00	169.0	53.6	82.4	31.3	151 ± 45
b	1.38	0.30	2.64	7.73	3.88	160.2	49.0	18.3	25.6	153 ± 42
c	2.04	0.45	2.23	7.12	3.47	180.3	48.0	0.0	0.0	145 ± 41
d	2.95	0.65	3.02	8.50	4.09	162.5	52.8	0.0	0.0	162 ± 49

of the complex permittivity increase with decreasing frequency. The filled samples on the other hand do not show a similar behavior. The relaxation occurring at low frequencies in PMMA is suppressed by the addition of nanoparticles. Further analysis of the dielectric data with the distribution of relaxation times [23–29] would indicate any (dis)similarities in the dielectric dispersions.

A numerical method based on the Monte Carlo method and constrained least-square technique was utilized to analyze the dielectric spectroscopy data [23]. The complex dielectric permittivity may be expressed in terms of a general distribution of relaxation times (DRT) formalism,

$$\varepsilon(\omega) = \varepsilon_\infty + (\varepsilon_s - \varepsilon_\infty) \int_{-\infty}^{\infty} \frac{g(\ln\tau)\,d\ln\tau}{1 + \imath\omega\tau} + \frac{\sigma_0}{\imath\varepsilon_0\omega}, \qquad (1)$$

where $\varepsilon_\infty \equiv \varepsilon'(\infty)$ and $\varepsilon_s \equiv \varepsilon'(0)$ (the quantity $\Delta\varepsilon \equiv \varepsilon_s - \varepsilon_\infty$ is defined as the dielectric relaxation amplitude), and $g(\ln\tau)$ is the distribution function. The parameters ω, τ, ε_0, and $\imath$ in (1) are the angular frequency, the relaxation time, the permittivity of the vacuum, and the pure complex number ($\imath \equiv \sqrt{-1}$). For a delta sequence distribution [30], (1) leads to a simple Debye response [31]. The method does not suffer from a priori assumptions as in parametric curve fitting techniques. In Fig. 4, one of the results of the analysis is illustrated. The sample with the 2 wt% $CoFe_2O_4$ filled PMMA shows several relaxation peaks. The numerical method can resolve the distribution over a larger time scale than the measuring system can acquire (shown with the dashed lines (– – –) in Fig. 4c). The peak appearing for times lower than 1×10^{-7} s is due to the numerical procedure. The material parameters, i.e., permittivity at high frequencies ε_∞ and dc conductivity σ_0, resolved from the DRT analysis are listed in Table 1. Notice that a deep analysis could not be possible in other dielectric data techniques based on the parametric methods (see the discussions in [24–27]).

Employing the DRT numerical method for the other samples highlights similarities between the dielectric dispersions of unfilled and filled samples, cf. Fig. 5. It appears there is a background relaxation with a time dependence in the form of a power law with $\tau^{0.2}$. There are small relaxation peaks between 10^{-6} s and 10^{-2} s that appear only in the filled samples. These extra relaxations are attributed to the interfacial region between the nanoparticles and the matrix, which is considered as the interaction zone by Nelson and co-authors [5, 6, 12]. In a previous paper, it has been reported that the method of DRT is sensitive in composites and could be able to resolve single relaxations [32, 33]. Here slightly similar behavior is observed, the relaxations which are present in all samples are marked with short vertical arrows in Fig. 5. The relaxation located at $\tau \sim 5 \times 10^6$ for the unfilled PMMA and the samples with low concentrations of

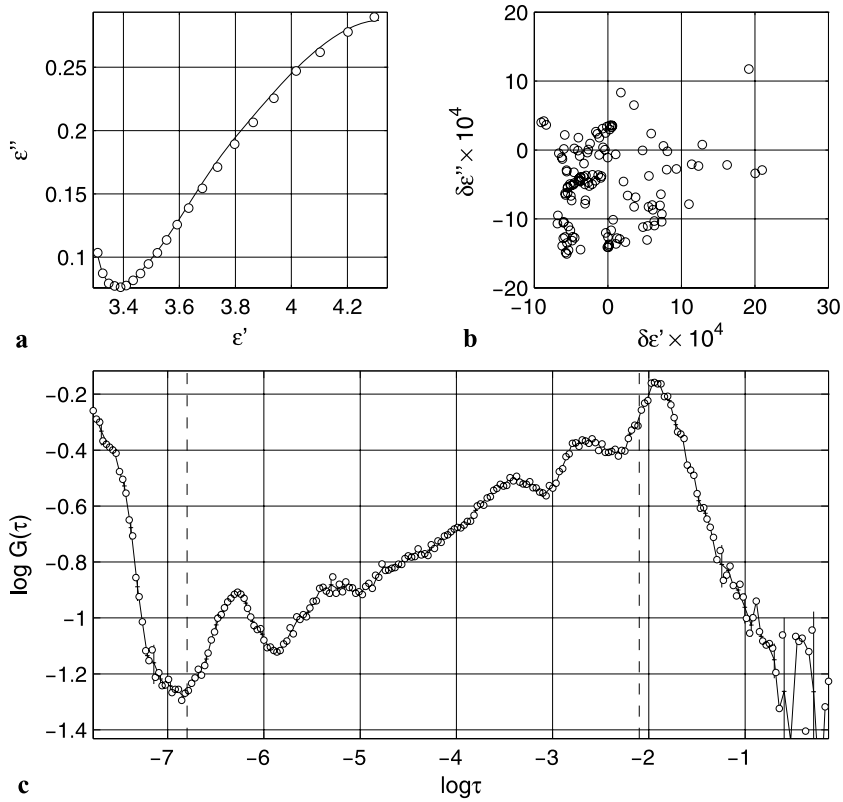

Fig. 4 **a** The Argand plot of the dielectric dispersion of sample with 2 wt% $CoFe_2O_4$. The *solid line* (——) is the curve fitted using the DRT in **c**. **b** The error in the real and the imaginary parts of the measured and estimated permittivity from the DRT, $\delta\varepsilon = \varepsilon_{mod} - \varepsilon_{est}$. **c** The DRT (*open symbols*-○) and the smoothed data is plotted with *solid lines* (——) and error bars. The *dashed lines* (– – –) in **c** illustrate the frequency limits (bounds) in the measurements corresponding to the DRT scale

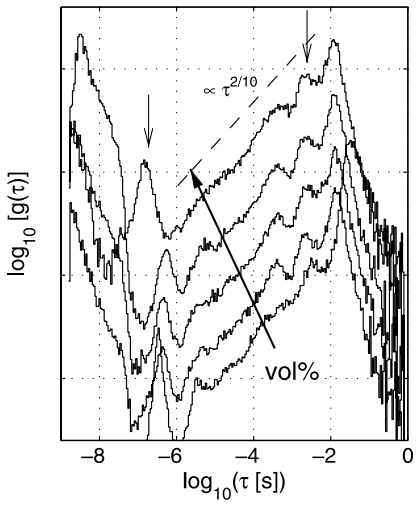

Fig. 5 The DRT spectra for unfilled and $CoFe_2O_4$ filled PMMA. The data are shifted up to guide the eyes, increasing concentration is shown with a *bold arrow*. The distribution peaks that are similar to all samples are marked with *vertical short arrows*. The DRT of samples indicate a time dependence $\tau^{2/10}$ on the time axis between 10^{-6} s and 10^{-2} s, this is shown with the *dashed line* (– – –)

$CoFe_2O_4$ moves a decade towards faster times for the sample with the highest $CoFe_2O_4$ concentration. In Fig. 3a, the shift in the real part of permittivity of PMMA is significant. As the nanoparticles are introduced to the system, the response at fast relaxations illustrate a different relaxation behavior compared to the unfilled PMMA. These relaxations could be due to the interfacial polarization [19, 34–36] since embedded metal oxide particles would yield a relaxation at high frequencies due to their intrinsic conductivity [19]. It is worth mentioning that these relaxations with fast times are not capable of generating large polarization response on the high frequency end of the dielectric dispersion. However, the particles somehow decreased the dielectric dispersion in PMMA at high frequencies, see ε_∞ in Table 1. The observation shows that molecular motion of polymer chains is blocked by the presence of nanoparticles lowering the permittivity of PMMA at high frequencies [2, 6, 11, 14–18], which is also an evidence of nanoconfinement discussed previously.

To investigate and confirm this observation, a further experiment was performed using a slowly varying electric field. A triangular voltage was applied, and the current through the samples was recorded. The current density versus electric field results are shown in Fig. 6a. The significance of the experimental results obtained for unfilled and 0.13 vol% $CoFe_2O_4$ filled PMMA are shown in Fig. 6b and 6c, respectively. The introduction of $CoFe_2O_4$ particles in PMMA reduces the conductivity and polarization effects in the material. If a material shows linear response in its conductivity and polarization, the response presented as in Fig. 6 should yield a deformed ellipse [37, 38]; none of the samples show this sort of behavior. The current densities

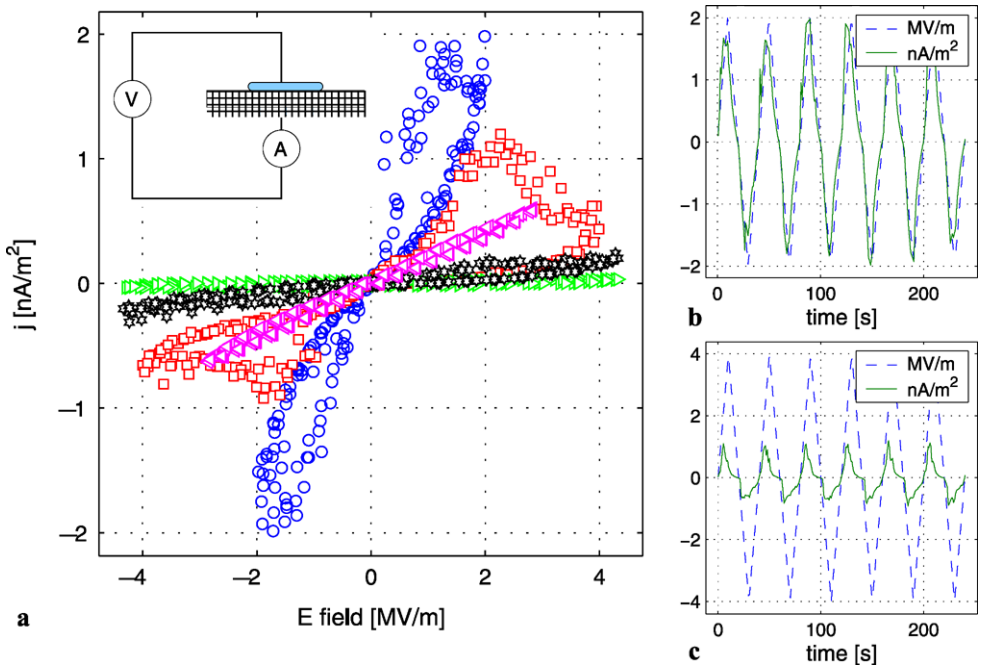

Fig. 6 **a** Current density versus applied electric field. Time dependent applied field and current density measured for **b** unfilled and **c** 0.13 vol% $CoFe_2O_4$ filled PMMA, respectively. The sample symbol labels are the same as in Fig. 3

illustrate that the response of the PMMA is altered from a non-linear to a more linear one with the nanoparticles. Moreover, polarization characteristics of PMMA changed with addition of nanoparticles, the displacement current response decreased significantly. Small signal conductivities estimated from the dielectric response using the DRT yield lower values than the unfilled PMMA as well, cf. Table 1.

Dielectric relaxation properties of insulating materials are of importance when the insulation is embedded in or in contact with another material, such as air, liquid nitrogen, transformer oil, etc., to form an insulation system. In that case dielectric permittivities of the macroscopic materials should be comparable to avoid electric field enhancement (electric stress) in the material with the lowest permittivity, which is typically air, liquid nitrogen or transformer oil in the insulation system. The nanodielectric materials studied here indicate that loading PMMA with a small amount of $CoFe_2O_4$ nanoparticles could encourage cryogenic power apparatus designers to consider filled PMMA in their applications instead of unfilled PMMA due to the significant decrease in the dielectric permittivity (approximately 60% at high frequencies and 20% at low frequencies, cf. sample c in Table 1). This last statement can be true only if the dielectric breakdown strength of the nanodielectrics are as good as the unfilled PMMA. To investigate the breakdown characteristics of unfilled and $CoFe_2O_4$ filled PMMA, a small number of samples, around 20, were tested in a liquid nitrogen bath to obtain statistical data on breakdown. Note that the high frequency permittivity values presented in Table 1 at room temperature would correspond to low frequency permittivity values at liquid nitrogen temperature.

In Fig. 7, the dielectric breakdown characteristics of the samples are presented as Weibull plots [39–42]. The Weibull statistics is based on an empirical survival probability $\mathsf{P}_s(x)$ [39, 40, 43],

$$\mathsf{P}_s(x) = 1 - \mathsf{F}(x), \tag{2}$$

where $\mathsf{F}(x)$ is the failure probability. The survival probability $\mathsf{P}_s(x)$ in (2) is given as follows [39]:

$$\mathsf{W}(x;\ A,\ B,\ x_\mathsf{W}) = \exp\left[-A(x - x_\mathsf{W})^B\right], \quad x \geq x_\mathsf{W}, \tag{3}$$

where parameters A, B, and x_W are fit parameters on the measurement of observables x. The authors of [44] emphasized the importance of plotting positions (median rank) using randomly generated data and compared their results for various plotting positions. In Benard median rank representation [45], the data is sorted from the lowest observable value to the highest one, and the indices i of the sorted observables are later used to assign the failure probability $\mathsf{F}(x_i)$ of the appropriate observed value x_i, as follows,

$$\mathsf{F}(x_i) = (i - 0.3)(N_d + 0.4)^{-1}, \tag{4}$$

where N_d is the total number of observables which was around 20 in the current study. Note that the data are sorted before the computation in (4). They are later analyzed as plotted in $\log_e\{\log_e[1 - \mathsf{F}(x_i)]^{-1}\}$ versus x_i or $\log_e(x_i)$; $\log_e$ is the natural logarithm. A nonlinear curve fitting (simplex) algorithm [46] shall yield the free parameters $\{A,\ B,\ x_\mathsf{W}\}$ in (3), where the significant engineering design parameter, the lower bound for the failure probability, is given by x_W.

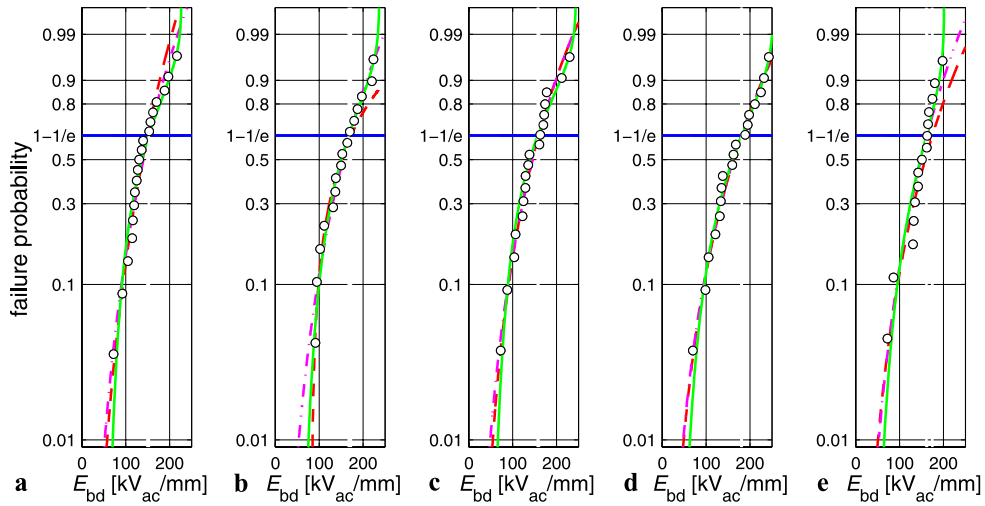

Fig. 7 Dielectric breakdown of unfilled **a** and $CoFe_2O_4$ filled PMMA samples **b–e** at liquid nitrogen (77 K). Samples **a** to **d** have breakdown data in subfigures **b** to **e**. The whole data sets are shown with the *filled symbols*. The data are analyzed with different failure statistics. Significant parameters of the models are listed in Table 1. The *solid* (——), *dashed* (– – –), and *dotted* (– · –) *lines* represent the data for (6), (3), and (5), respectively. Sample thicknesses were around 20–50 µm

The two parameter Weibull distribution assumes that the lower bound $x_W \equiv 0$. This expression is also considered in the present study, and its survival probability P_s is given as

$$w(x;\ a,\ b) = \exp\left[-(x/a)^b\right]. \tag{5}$$

The parameters a, and b are obtained from a linear curve fitting algorithm using the $\log_e$-linear scale. The parameter a is the 63% $(1 - 1/e)$ failure probability of a sample. We list an additional parameter a_1 in Table 1 which is the 1% failure probability of the sample.

Since the Weibull expression in (3) is an empirical expression, another, more suitable expression can also be adapted as the failure probability $F(x)$ for a given data set. We therefore propose an exponential function for the failure probability as follows:

$$G(x;\ \alpha,\ \beta,\ x_G) = \alpha x^{-1} \exp\left[-\beta(x - x_G)^{-1}\right],$$
$$x \geq x_G, \tag{6}$$

where the free parameters α, β, and x_G are acquired as before using the simplex (direct search) method [46]. In (6), x_G is similar to x_W such that it is also the lower bound (threshold) value for the failure probability.

The breakdown data were analyzed with the presented expressions as shown in Fig. 7. The results of the statistical analysis are listed in Table 1, only two-parameter Weibull expression is able to represent the all composite data sets. Other two expressions, (3) and (6), do not yield threshold values for the uncensored data. However, censoring [41] or the application of a novel numerical method [42] might yield a threshold value for the samples, which is not included in the current presentation. The inclusion of $CoFe_2O_4$ nanoparticles improves the dielectric breakdown characteristics of the PMMA. The amount of $CoFe_2O_4$ employed increased the mean value of the breakdown strength from 140 kV/mm to 163 kV/mm depending on the concentration of $CoFe_2O_4$. The slopes of the Weibull plots β are not different for the samples, while their 63% breakdown values α indicate a similar behavior as μ. The three-parameter Weibull expressions was not able to generate a workable parameter for the data sets. However, (6) produced better fits for the data however its threshold values were not better than the unfilled PMMA, cf. Table 1. As a result the PMMA doped with $CoFe_2O_4$ is as good as (or slightly better than) the unfilled PMMA. A similar observation has been reported for oil-based magnetic fluids in which the addition of maghemite nanoparticles increased the dielectric breakdown of transformer oil [47]. Consequently, slightly $CoFe_2O_4$ filled PMMA can be utilized as an electrical insulation material at low temperatures in high voltage applications or power apparatus.

To further investigate the dielectric behavior of nanodielectrics, two dimensional numerical calculations were performed using the effective medium theory (see the details in [19, 48–50]). In the calculations frequency dependent properties of the phases are disregarded. It is observed that the coated nanoparticles help to grade the potential distribution uniformly in a composite. In the numerical analysis the nanodielectric structure presented in Fig. 1b was taken into consideration, and only a particle cluster region was employed in the calculations as shown in Fig. 8a. The particles were represented as hexagons with sides a. The surfactant region (shown with thick lines in Fig. 8a), interphase between the particles, has dimensions of $0.2a$. The material parameters were assigned as matrix ε_1, particles ε_2 and surfactant ε_3. The fraction of the different material regions were 0.44, 0.36, and 0.20 for the matrix, particles and interphase, respectively. The permittivity of the matrix was taken

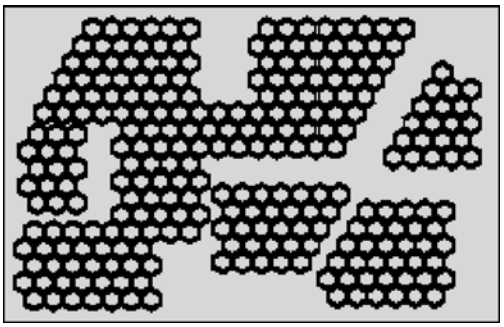

a

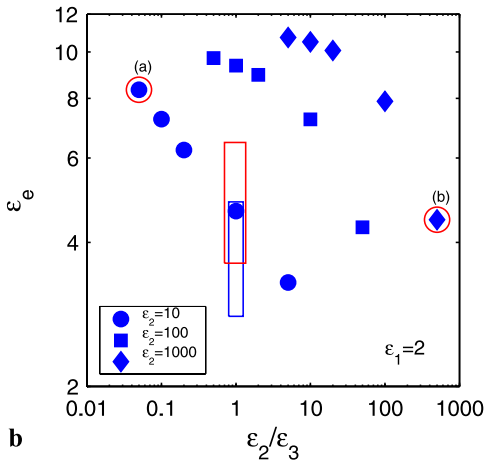

b

Fig. 8 **a** The geometry considered in the two dimensional numerical calculations based on the finite element method. The geometry represents the region where particles form clusters. Each particle is assumed to be covered with a layer which can be considered as a surfactant or the matrix material. **b** The effective dielectric permittivities calculated for some phase permittivity configurations as a function of ratio of permittivity of particles to interphase. In the calculations a composite with three components, ε_i with $i = 1, 2, 3$, are considered. The matrix phase, inclusions and interphase are denoted by 1, 2, and 3, respectively. The rectangular regions represents the bounds expected for the particle concentrations with and without the layers included in the calculations. The data points labeled with '(a)' and '(b)' are the values calculated from the field distributions in Fig. 9

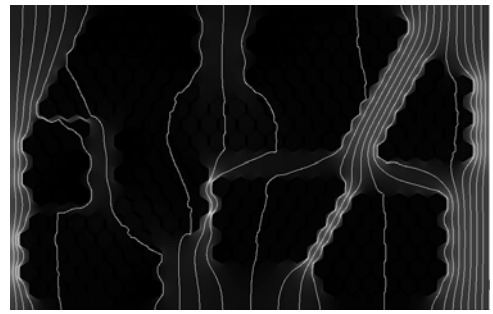

a

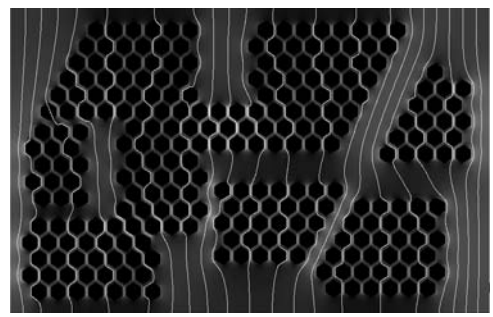

b

Fig. 9 Electrical field (*gray* scale) and equi-potential (*solid lines* ——) distributions in the composite structure for two of the cases represented in Fig. 8 with '(a)' and '(b)'. *Light gray* regions indicate the high electric field regions. **a** The interphase has higher dielectric permittivity than the matrix medium one. **b** The interphase has the same dielectric permittivity as the matrix. In **a**, particles are aggregated and deform the potential and electric field significantly causing large electric field values. In **b**, on the contrary observe that individual particles are visible when particles are separated which improves the potential distribution because each particle acts like a floating electrode and smooths out the voltage distribution. These two distributions clearly illustrate that small particles have field grading properties when they are separated with a low permittivity (permittivity close to the matrix medium one) interphase/surfactant material

to be constant, $\varepsilon_1 = 2$. The permittivity of $CoFe_2O_4$ particles were taken from the literature, where it was reported for different firing temperatures and grain sizes [51, 52], $\varepsilon = [6 - 25]$. Here we considered three different values to indicate the significance of the surfactant layer. The permittivity of surfactant, oleic acid, was taken from the literature [53, 54], $\varepsilon_3 \sim 2$. Again several surfactant permittivity values were considered to once again show the importance of electrical properties of the surfactant on the effective permittivity. Figure 8b shows the expected permittivity ε_e for the particle cluster. It is very clear that when the permittivity of the surfactant ε_3 is lower than the particles permittivity ε_2 and close to the matrix permittivity ε_1, the region in which particles aggregated have an effective permittivity not much different than the matrix permittivity, $\varepsilon_e \sim 2 \times \varepsilon_1$. Notice that even high permittivity particles would not yield a high effective permittivity for clusters. This effect would be also obvious if dielectric mixture expressions and depolarization factors of different shapes are taken into consideration. A surfactant with a high permittivity would yield a high effective permittivity. As a result the permittivity values ε_∞ listed in Table 1 can be better understood with the current numerical findings. Low dielectric permittivity of the oleic acid and broken connectivity of the particles yield low permittivity values for the nanodielectrics.

To better visualize the surfactant effect, two field distributions are plotted in Fig. 9. In Fig. 9a, the equi-potential lines are not distributed uniformly, and the electric field distribution, presented with a gray scale, has no component inside the particles (as shown with a solid black region) when the surfactant has high dielectric permittivity. However, Fig. 9b illustrates the potential distribution uniformity

and field distribution where the region between particles are stressed when the surfactant has a similar permittivity value as the matrix material. Since there is a relation between dielectric breakdown and thickness in insulation materials it is anticipated that the field would not be high enough to cause a breakdown between particles. This might be a reason why high dielectric breakdown values are observed in nanodielectrics.

In conclusion, we reported our findings on the dielectric properties and breakdown characteristics of $CoFe_2O_4$ filled PMMA nanodielectrics. It was observed that a slight enhancement in the breakdown strength can be obtained by introducing spherical mono dispersed $CoFe_2O_4$ nanoparticles. A significant decrease (60%) in the dielectric permittivity of the nanocomposite was recorded compared to the unfilled PMMA. The samples prepared with low concentration of $CoFe_2O_4$ ($\leq$1 vol% or <3 wt%) indicate improved properties as an electrical insulation material for cryogenic applications, e.g., high temperature superconducting cable systems. Here it has once again been shown that metal oxide inclusions in nanoparticle form can be employed as an alternative to voltage stabilizing agents to improve the dielectric strength of polymeric materials. Furthermore, a couple of points are introduced to explain the dielectric properties of nanocomposites by utilizing numerical calculations. It is manifested that employing a surfactant with low dielectric permittivity yields a low effective dielectric permittivity of nanodielectric mixtures due to broken connectivity between particles independent of the permittivity of the nanoparticles.

References

1. E. Tuncer, I. Sauers, D.R. James, A.R. Ellis, M.P. Paranthaman, A. Goyal, K.L. More, Nanotechnology **18**, 325704 (2007)
2. E. Tuncer, I. Sauers, D.R. James, A.R. Ellis, M.P. Paranthaman, T. Aytuğ, S. Sathyamurthy, K.L. More, J. Li, A. Goyal, Nanotechnology **18**, 025703 (2007)
3. E. Tuncer, I. Sauers, D.R. James, A.R. Ellis, R.C. Duckworth, IEEE Trans. Dielectr. Electr. Insul. **15**(1), 236 (2008)
4. E. Tuncer, R.C. Duckworth, I. Sauers, D.R. James, A.R. Ellis, in *CEIDP'07 2007 Annual Report*. Conference on Electrical Insulation and Dielectric Phenomena (IEEE Dielectrics and Electrical Insulation Society, 2007), pp. 225–227
5. J.K. Nelson, J.C. Fothergill, Nanotechnology **15**, 586 (2004)
6. J.K. Nelson, Y. Hu, J. Phys. D: Appl. Phys. **38**, 213 (2005)
7. Q. Tan, P. Irwin, Y. Cao, IEE J. Trans. FM **126**(11), 1153 (2006)
8. Y. Cao, P.C. Irwin, K. Younsi, IEEE Trans. Dielectr. Electr. Insul. **11**(5), 797 (2004)
9. T. Tanaka, IEEE Trans. Dielectr. Electr. Insul. **12**(5), 914 (2005)
10. Y. Uozumi, Y. Kikuchi, N. Fukumoto, M. Nagata, Y. Wakimoto, T. Yoshimitsu, in *CEIDP'07 2007 Annual Report*. Conference on Electrical Insulation and Dielectric Phenomena (IEEE Dielectrics and Electrical Insulation Society, 2007), pp. 228–231
11. S. Gross, D. Camozzoa, V.D. Notoa, L. Armelaoa, E. Tondello, Eur. Polym. J. **43**(3), 673 (2007)
12. R.C. Smith, C. Liang, M. Landry, J.K.N.L.S. Schadler, IEEE. Trans. Dielectr. Electr. Insul. **15**(1) (2008)
13. T.J. Lewis, J. Phys. D: Appl. Phys. **38**, 202 (2005)
14. D. Fragiadakis, E. Logakis, P. Pissis, V.Y. Kramarenko, T.A. Shantalii, I.L. Karpova, K.S. Dragan, E.G. Privalko, A.A. Usenko, V.P. Privalko, vol. 10 (IOP, 2005), pp. 139–142
15. R.D. Priestley, P. Rittigstein, L.J. Broadbelt, K. Fukao, J.M. Torkelson, J. Phys: Condens. Matter **19**, 205120 (2007), 12pp
16. R.D. Priestley, C.J. Ellison, L.J. Broadbelt, J.M. Torkelson, Science **309**(5733), 456 (2005)
17. I. Kalogeras, E. Neagu, Eur. Phys. J. E—Soft Matter **14**(2), 193 (2004)
18. W.T.S. Huck, Chem. Commun. **33**, 4143 (2005)
19. E. Tuncer, Y.V. Serdyuk, S.M. Gubanski, IEEE Trans. Dielectr. Electr. Insul. **9**(5), 809 (2002)
20. C. Brosseau, A. Beroual, Prog. Mater. Sci. **48**, 373 (2003)
21. A. Sihvola, *Electromagnetic Mixing Formulas and Applications*. IEE Electromagnetic Waves Series, vol. 47 (The Institute of Electrical Engineers, London, 1999)
22. A.J. Rondinone, A.C.S. Samia, Z.J. Zhang, J. Phys. Chem. B **103**, 6876 (1999)
23. E. Tuncer, S.M. Gubański, IEEE Trans. Dielectr. Electr. Insul. **8**, 310 (2001)
24. E. Tuncer, R.J. Macdonald, J. Appl. Phys. **99**, 074106 (2006)
25. E. Tuncer, M. Wegener, R. Gerhard-Multhaupt, J. Non-Cryst. Solids **351**(33-35), 2917 (2005)
26. E. Tuncer, M. Wegener, P. Frübing, R. Gerhard-Multhaupt, J. Chem. Phys. **122**, 084901 (2005)
27. E. Tuncer, M. Furlani, B.-E. Mellander, J. Appl. Phys. **95**(6), 3131 (2004)
28. J.R. Macdonald, J. Comput. Phys. **157**, 280 (2000)
29. J.R. Macdonald, J. Chem. Phys. **102**, 6241 (1995)
30. E. Butkov, *Mathematical Physics*. Addison-Wesley Series in Advanced Physics (Addison-Wesley, Menlo Park, 1968)
31. P. Debye, *Polar Molecules* (Dover Publications, New York, 1945)
32. E. Tuncer, N. Bowler, I.J. Youngs, K.P. Lymer, Philos. Mag. **86**, 2359 (2006)
33. E. Tuncer, G.A. Niklasson, Opt. Commun. **281**(17), 4374 (2008)
34. J.C. Maxwell, *A Treatise on Electricity and Magnetism*, vol. 1, 3rd edn. (Clarendon Press, Oxford, 1891), pp. 450–464, reprint by Dover
35. K.W. Wagner, Arch. Electrotech. **II**(9), 371 (1914)
36. R. Sillars, J. Inst. Electr. Eng. **80**, 378 (1937)
37. E. Tuncer, S.M. Gubański, Turk. J. Phys. **26**, 1 (2002)
38. E. Tuncer, Licenciate thesis—Tech. rep. 338 L, Department of Electric Power Eng., Chalmers University of Technology, Gothenburg, Sweden, 2000
39. W. Weibull, J. Appl. Mech. **18**, 293 (1951)
40. W. Weibull, *A Statistical Theory of the Strength of Materials*. Ingeniörsvetenskapsakademiens Handlingar, vol. 151 (Generalstabens Litografiska Anstalts, Stockholm, 1939)
41. S.M. Rowland, R.M. Hill, L.A. Dissado, J. Phys. C: Solid State Phys. **19**, 6263 (1986)
42. E. Tuncer, I. Sauers, D.R. James, A.R. Ellis, M.O. Pace, J. Phys. D: Appl. Phys. **39**, 4257 (2006)
43. E.J. Gumbel, *Statistics of Extremes* (Columbia University Press, New York, 1958)
44. S.W. Looney, T.R. Gulledge Jr., Statistician **34**(3), 297 (1985)
45. A. Benard, E. Bos-Levenbach, Stat. Neerlandica **7**, 163 (1953), translation in English can be found on http://www.barringer1.com/wa_files/The-plotting-of-observations-on-probability-paper.pdf
46. J.A. Nelder, R. Mead, Comput. J. **7**, 308 (1965)
47. P.P.C. Sartoratto, A.V.S. Neto, E.C.D. Lima, A.L.C. Rodrigues de Sá, P.C. Morais, J. Appl. Phys. **97**, 10Q917 (2005)
48. E. Tuncer, Turk. J. Phys. **27**, 121 (2003). arXiv:cond-mat/0107384
49. E. Tuncer, S.M. Gubański, B. Nettelblad, J. Appl. Phys. **89**(12), 8092 (2001)

50. E. Tuncer, B. Nettelblad, S.M. Gubański, J. Appl. Phys. **92**(8), 4612 (2002)
51. M. George, S.S. Nair, K.A. Malini, P.A. Joy, M.R. Anantharaman, J. Phys. D: Appl. Phys. **40**, 1593 (2007)
52. C.R. Vestal, Final Report AFRL-ML-WP-TR-2006-4209, Air Force Research Laboratory, Dayton, OH, 2006
53. P.C. Fannin, C.N. Marin, I. Malaescu, N. Stefu, J. Phys.: Condens. Matter **19**, 036104 (2007), 8pp
54. S.R. Smith, K.R. Foster, Phys. Med. Biol. **30**(9), 965 (1985)